Biosensors and Bioelectronics 190 (2021) 113411

Contents lists available at ScienceDirect

Biosensors and Bioelectronics

journal homepage: www.elsevier.com/locate/bios

Highly permselective uric acid detection using kidney cell membrane–functionalized enzymatic biosensors

Insu Kim [a,1], Young Im Kim [b,1], Sang Won Lee [a], Hyo Gi Jung [a,c], Gyudo Lee [d,e,**], Dae Sung Yoon [a,c,*]

[a] School of Biomedical Engineering, Korea University, Seoul, 02841, South Korea
[b] Department of BioNano Technology, Gachon University, Seongnam, 13120, South Korea
[c] Interdisciplinary Program in Precision Public Health, Korea University, Seoul, 02841, South Korea
[d] Department of Biotechnology and Bioinformatics, Korea University, Sejong, 30019, South Korea
[e] Interdisciplinary Graduate Program for Artificial Intelligence Smart Convergence Technology, Korea University, Sejong, 30019, South Korea

ARTICLE INFO

Keywords:
Electrochemical detection
Uric acid biosensor
Kidney cell membrane
Urate transporter 1
Permselectivity
Uric acid oxidase

ABSTRACT

Abnormal blood uric acid (UA) levels can lead to its crystallization in the joints, consequently resulting in gout. Accurate detection of UA in the blood is imperative for the early diagnosis of gout. However, electrochemical UA biosensors are vulnerable to antioxidants in the blood, limiting accurate UA detection. To address this issue, we focused on the function of uric acid transporter 1 (URAT1), which is selectively permeable to UA. URAT1 is abundant in the kidney cell membrane (KCM). To apply URAT1 to a sensor, we developed a KCM-coated UA biosensor (called the KCM sensor) that could selectively detect UA through URAT1. The KCM coating in the fabricated KCM sensor was verified via scanning electron microscopy, atomic force microscopy, and confocal microscopy. The KCM sensor enabled the detection of UA in the range of 0–1000 μM, with a limit of detection of 8.5 μM, suggesting that it allows the diagnosis of the early stages of gout. On the other hand, the UA permeability of the KCM sensor was significantly reduced in the presence of a URAT1 inhibitor, implying that URAT1 is a key factor for UA detection. The selectivity of the KCM sensor was demonstrated by measuring the amount for UA in the presence of various antioxidants. Finally, the KCM sensor was capable of measuring UA in human serum and was reproducible with 0.5–1.6% deviation. The UA permeability and selectivity of the KCM sensor were maintained even after 3 weeks of storage.

1. Introduction

Uric acid (UA) is the final decomposition product from the metabolism of purine, a constituent of nucleic acids, in the liver and is present in meat products. The blood UA level is regulated by the nephrological system, which excretes UA through the kidney. High UA (~350 μM) level could lead to gout, a condition characterized with the precipitation of needle-like UA crystals in the joints, skin, and other tissues, that is common in patients with diabetes, Lesch–Nyhan disease, Down syndrome, and Von Gierke disease (Abou-Elela, 2017). The incidence of gout has increased in recent decades (Singh et al., 2019).

Identification of UA crystals is imperative for the diagnosis of gout. At present, two methods, polarized light microscopy and X-ray imaging, are employed to detect UA crystals. UA crystals can be visually detected from the synovial fluid via polarized light microscopy, but sampling of the synovial fluid can be painful. X-ray imaging, on the other hand, allows non-invasive observation of UA crystals. These methods are expensive and require large equipment and some specialists. Furthermore, UA crystals can be detected only at the acute stage of gout, which is associated with painful intercritical segments from excessive UA crystal deposition in the joints. Thus, it is difficult to have an early diagnosis of gout using conventional methods (Vaidya et al., 2018).

To overcome these limitations, UA biosensors have been developed. Hyperuricemia, an early symptom of gout, can be detected using UA biosensors. Electrochemical UA detection has various advantages, such as early diagnosis, rapid measurement, high sensitivity, portable size,

* Corresponding author. School of Biomedical Engineering, Korea University, Seoul, 02841, South Korea.
** Corresponding author. Department of Biotechnology and Bioinformatics, Korea University, Sejong, 30019, South Korea.
E-mail addresses: lkd0807@korea.ac.kr (G. Lee), dsyoon@korea.ac.kr (D.S. Yoon).
[1] These authors contributed equally to this manuscript.

https://doi.org/10.1016/j.bios.2021.113411
Received 4 April 2021; Received in revised form 30 May 2021; Accepted 3 June 2021
Available online 5 June 2021

and ease of use (Mathew et al., 2021). Therefore, electrochemical enzymatic biosensors for sensitive UA detection have been constructed using nanomaterials composed of copper oxide, graphene oxide, and zinc oxide (Krishnan et al., 2019).

Despite their superior sensitivity, electrochemical UA biosensors are often easily interfered by antioxidants in the blood, such as lipoic acid, glutathione, and vitamins. Therefore, it is important to improve the selectivity of electrochemical UA biosensors for accurate UA detection. UA is selectively reabsorbed through uric acid transporter1 (URAT1) in the kidney to regulate its excretion. URAT1 is localized in the apical membrane of the kidney proximal tubular cells. It has been reported that cell membranes and membrane proteins can be functionalized onto various nanoparticles and solid surfaces to provide various functionalities, such as the selective transportation of molecules through the membrane (Stiburkova et al., 2019). Applying a URAT1-rich kidney cell membrane (KCM) on UA biosensors could potentially increase the selectivity of UA against antioxidants that cannot permeate the KCM (Kim et al., 2018).

In this study, we fabricated a uric acid oxidase (UOx)-immobilized sensor (called the UOx sensor) and a KCM-coated UOx sensor (called the KCM sensor). The surface morphology of the KCM sensor was verified via scanning electron microscopy (SEM), atomic force microscopy (AFM), and confocal microscopy, and its electrochemical properties were studied using cyclic voltammetry (CV). The sensing performance of the KCM sensor was confirmed to be in the range of 0–1000 μM UA. Its selectivity was demonstrated by testing five antioxidants in human plasma (Shindyapina et al., 2017). Finally, the feasibility, stability, and reproducibility of the KCM sensor were verified by evaluating its practical applications. Taken together, we demonstrate the development of a kidney-mimetic electrochemical biosensor functionalized with URAT1 to improve the accuracy of UA detection.

2. Material and methods

2.1. Materials and reagents

Screen-printed carbon electrodes (SPCEs, DRP–110) were purchased from DropSens. Nafion 117 (Naf), ferrocene (Fc), potassium ferricyanide ($[Fe(CN)_6]^{3-}$), potassium ferrocyanide ($[Fe(CN)_6]^{4-}$), potassium chloride (KCl), UOx, glutaraldehyde, ascorbic acid (AA), barbituric acid (BA), lipoic acid (LA), glutathione (GSH), niacinamide (NA), protease and phosphatase inhibitor cocktail, fetal bovine serum (FBS), bovine serum albumin (BSA), and penicillin–streptomycin G were purchased from Sigma-Aldrich. Phosphate-buffered saline (PBS, pH 7.4), Dulbecco's modified Eagle's medium (DMEM), and distilled water were purchased from Gibco, and 18:1 PE-CF (1,2–dioleoyl–sn–glycero–3–phosphoethanolamine–N–(carboxyfluorescein) [ammonium salt]) and 18:1 PC (cis) (1,2–dioleoyl–sn–glycero–3–phosphocholine) (DOPC) were purchased from Avanti Polar Lipids. The URAT1 inhibitors (verinurad) were purchased from ChemScene. In the selectivity test, each antioxidant (40 μM) was added to 400 μM UA solution. All the chemicals were freshly prepared prior to the experiments.

2.2. Instrumentation

The electrochemical characteristics of each sensor (bare, UOx, and KCM sensors) were analyzed using CV (VersaSTAT3, Princeton Applied Research, CA, USA). Electrochemical characterization was performed in PBS (pH 7.4) containing 0.2 M KCl and 10 mM $[Fe(CN)_6]^{3-/4-}$. CV was conducted in the potential range of −0.3 to 0.6 V and a scan rate of 10–100 mV/s. The topology of each sensor was measured using a non-contact mode atomic force microscope (AFM, NX-10, Park Systems, Republic of Korea) using a cantilever with a force constant of 42 N/m and a resonant frequency of 330 kHz (NCHR, Nanosensors, Switzerland). The surface of each sensor was visualized using a scanning electron microscope (SEM, JEOL, JSM-6701F, Japan). The diameters of the KCM vesicles were measured using a Zetasizer (Nano S90, Malvern Panalytical, UK). The zeta potential was measured using a zeta potential analyzer (ELSZ-1000, Otsuka Electronics, Japan). Fluorescence images were obtained using a fluorescence (18:1 PE CF)-labeled KCM sensor (IX81, Olympus, Japan).

2.3. Kidney cell culture and KCM extraction

Human embryonic kidney cells (HEK293) were purchased from the Korean Cell Bank and cultured in minimum essential medium (MEM) with 10% FBS and 1% penicillin–streptomycin at 37 °C in a 5% CO_2 incubator. Kidney cells were collected via centrifugation at 200×*g* for 5 min and washed three times with PBS. The cells were suspended in PBS containing proteinase and phosphatase inhibitor cocktail to prevent the degradation of membrane proteins and phospholipids. Next, the kidney cells were lysed using a homogenizer (7000 rpm, 15 passes). The lysate containing the KCM and cellular organelles was centrifuged at 800×*g* for 5 min. The supernatant was centrifuged at 20,000×*g* for 5 min to separate the KCM from cellular organelles. The sediments, purified KCM, and membrane proteins were collected and stored in a deep freezer (−80 °C) until analysis (Jo et al., 2019; Lee et al., 2021).

2.4. Preparation of KCM sensor

The working electrodes of the SPCE were electrochemically activated via CV using 0.5 M sulfuric acid to eliminate the passivating layer (Shi and Shiu, 2001; Wang et al., 1996). The potential was cycled 12 times from −0.4 to 1.4 V (vs. Ag/AgCl) at a scan rate of 200 mV/s to achieve a stable voltammogram. This cycling did not affect the Ag electrode (Price et al., 1986). Fc (5 mg) was added to 1 mL of 5% Naf (Fc-Naf). Fc-Naf was cast on the working electrode (2 μL) and dried. Here, Fc was physically entrapped by the Naf thin film. As a result, Fc was prevented from diffusion during fabrication (Ghosh et al., 2015; Yan et al., 2020). To form the UOx layer, a UOx mixture containing 10 mg/mL UOx, 8.0 mg/mL BSA, and 1.25% glutaraldehyde was cast on the working electrode and dried at room temperature. The modified electrode was washed with PBS to remove the unbound UOx. Then, the KCM concentrate was diluted to 0.5% using PBS to prepare the KCM solution. The KCM solution was sonicated for 5 min to produce KCM vesicles. The vesicles were coated onto the UOx layer using the vesicle fusion method (Fig. S1) at 37 °C for 30 min. The vesicles were disrupted and coated onto a solid surface in the form of a lipid bilayer. After incubation, the sensor was dried at room temperature for 2 h (Perry et al., 2006).

3. Result and discussion

3.1. Fabrication of KCM sensor

The working electrode of the SPCE was serially functionalized with the Fc-Naf and UOx mixture. Fc is widely used as an electronic mediator because it can promote stable electron transfer. To detect UA, the following chemical reactions occurred:

$$Fc - e^- \rightarrow Fc^+ \quad (1)$$

$$Uric\ acid + O_2 \xrightarrow{UOx} Allatoin + CO_2 + 2H^+ + 2e^- \quad (2)$$

$$Fc^+ + e^- \rightarrow Fc \quad (3)$$

Equations (1)–(3) represent electrochemical oxidation, Fc oxidation, and electrochemical reduction, respectively.

KCM was diluted in PBS and sonicated for 5 min to produce KCM vesicles. The diameter and zeta potential of the KCM vesicles were 100–200 nm and 19.46 mV, respectively (Fig. S2). To optimize UA permeation, we functionalized various concentrations of KCM vesicles (0–1%) onto a UOx sensor (Fig. S3). The permeability of the UOx sensor

coated with 1% KCM was the lowest, leading to a decrease in the cathodic peak current (I_{pc}) by 23.5–62% of the intensity reported for the UOx sensor. On the other hand, the UOx sensor coated with 0.5% KCM showed a permeability similar to that of the UOx sensor without KCM. These results indicated that the presence of URAT1 on the KCM increased its permeability to UA (Scheme 1). We then verified the optimal temperature for the KCM coating with 200 μM UA. The KCM sensor coated at 37 °C showed an I_{pc} of 10.5 μA, which was 98% higher than that of the UOx sensor (Fig. S4). The KCM sensor coated at 50 °C showed an I_{pc} of 9.4 μA, which was 87.4% higher than that of the UOx sensor. Therefore, we optimized the temperature for KCM sensor fabrication to be 37 °C.

3.2. Surface visualization and topological analysis of the KCM sensor

The morphologies of the bare, UOx, and KCM sensors were analyzed using AFM and SEM (Fig. 1). To investigate each coating, the arithmetic average roughness (Ra) of the surface of each sensor was calculated using the following equation:

$$\mathrm{Ra} = \frac{1}{l}\int_0^l |z(x)|dx \tag{4}$$

where l and z(x) represent the evaluation length and profile height function, respectively.

The Ra of bare, UOx, and KCM sensors were 38.2 ± 7.7, 58.2 ± 7.4, and 34.3 ± 3.6 μm, respectively (Fig. S5). It was verified that the surface of the working electrode (i.e., glassy carbon) on the bare sensor became 1.5-fold rougher after UOx immobilization. However, the KCM coating made the surface of the working electrode smoother, similar to that of the bare sensor. As a result, the Ra of the KCM sensor decreased by 41% compared to that of the UOx sensor. This observation was confirmed through the SEM images obtained. We also verified the presence of the KCM coating using confocal microscopy (Fig. S6). Fluorescence-labeled phospholipids were intercalated into the KCM vesicles. The fluorescence-labeled KCM sensor was fabricated, and the presence of the KCM layer was verified using fluorescence imaging (Hedegaard et al., 2018).

3.3. Electrochemical characterization of the KCM sensor

The electrochemical properties of the KCM sensors were investigated through CV. Fig. 2A shows the CV curves of the bare, UOx, and KCM sensors at a scan rate of 50 mV/s and a scan range of −0.2 to 0.6 V. The I_{pc} of these sensors were 120.8, 72.6, and 58.9 μA and their anodic peak currents (I_{pa}) were −136.18, −89.3, and −76.9 μA, respectively. The I_{pc} values of the UOx and KCM sensors were reduced by 40% and 51%, respectively, compared to that of the bare sensor. We verified that the UOx and KCM coatings retarded the electron transfer capability of the sensor (RoyChoudhury et al., 2018). We then investigated the effects of the scan rate on the peak current using a KCM sensor (Fig. 2B and C). The I_{pc} and I_{pa} versus the root-mean-squared scan rate were highly linear, with regression coefficients (R^2) of 0.999 and 0.9934, respectively. The Randles-Sevcik equation demonstrated that this result provides evidence for a chemically reversible redox process (Elgrishi et al., 2018).

3.4. Verification of URAT1 on the KCM sensor

To verify the UA permeability of the KCM, we compared the sensing performance of the KCM sensor with that of the UOx sensor and a phospholipid bilayer–coated sensor (DOPC sensor). Here, DOPC was employed as a substitute for KCM without membrane proteins (Fig. S7). The UA-sensing performance of each sensor was analyzed through CV (Fig. 3A–C). Fig. 3D shows the I_{pc} of each sensor versus the UA concentration. The UOx and KCM sensors showed similar electrochemical tendencies, and their I_{pc} linearly increased with the concentration of UA ($R^2 = 0.9989$, and 0.9993, respectively). However, the DOPC sensor was unable to detect UA because DOPC layers prevented UA permeation (Bacellar et al., 2018).

To confirm UA permeability on the KCM sensor via URAT1, we inhibited URAT1 in the KCM (Fig. 4A). Verinurad, a URAT1 inhibitor, binds to the residues of URAT1 (Ser-35, Phe-365, and Ile-481). Once the inhibitor binds to URAT1, UA cannot be transported through KCM anymore (Perry et al., 2006; Tan et al., 2017). The KCM vesicles were incubated with 40 μM verinurad for 60 min (Fitz-Patrick et al., 2018). The URAT1-blocked KCM vesicles were then coated onto a UOx sensor (URAT1-blocked KCM sensor). The I_{pc} of the KCM and URAT1-blocked KCM sensors with 400 μM UA were 15.678 and 13.2 μA, respectively. Thus, the I_{pc} of the URAT1-blocked KCM sensor decreased by 15.8% compared to that of the KCM sensor. These results confirm that URAT1 is a key factor for enabling the permselective detection of the KCM sensor to UA.

3.5. Selectivity test

To demonstrate the UA selectivity of the KCM sensor, we tested the electrochemical reaction of the KCM sensor by adding various antioxidants to the UA solution (Fig. 4B). Human serum is rich in the five

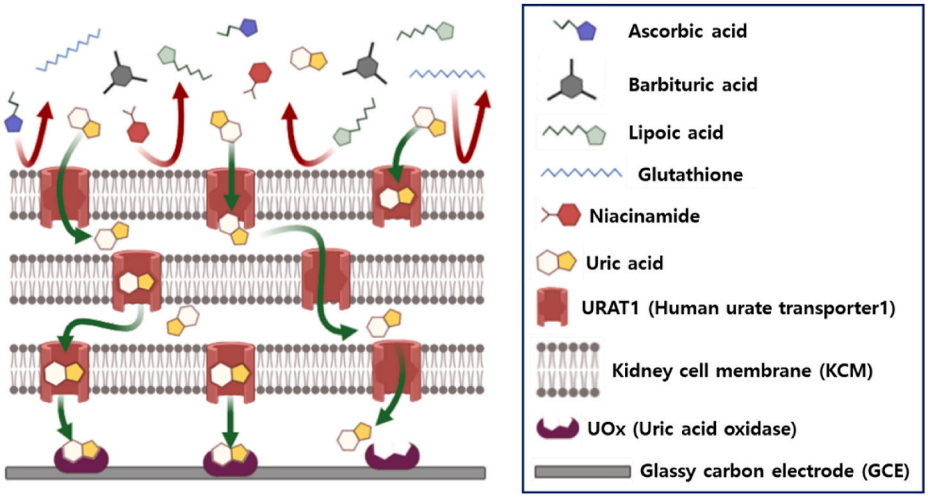

Scheme 1. Working mechanism of the KCM sensor. The KCM layers are coated onto the UOx-immobilized sensor. The KCM works as a selective filter, selectively transporting UA via URAT1 and preventing the permeation of antioxidants.

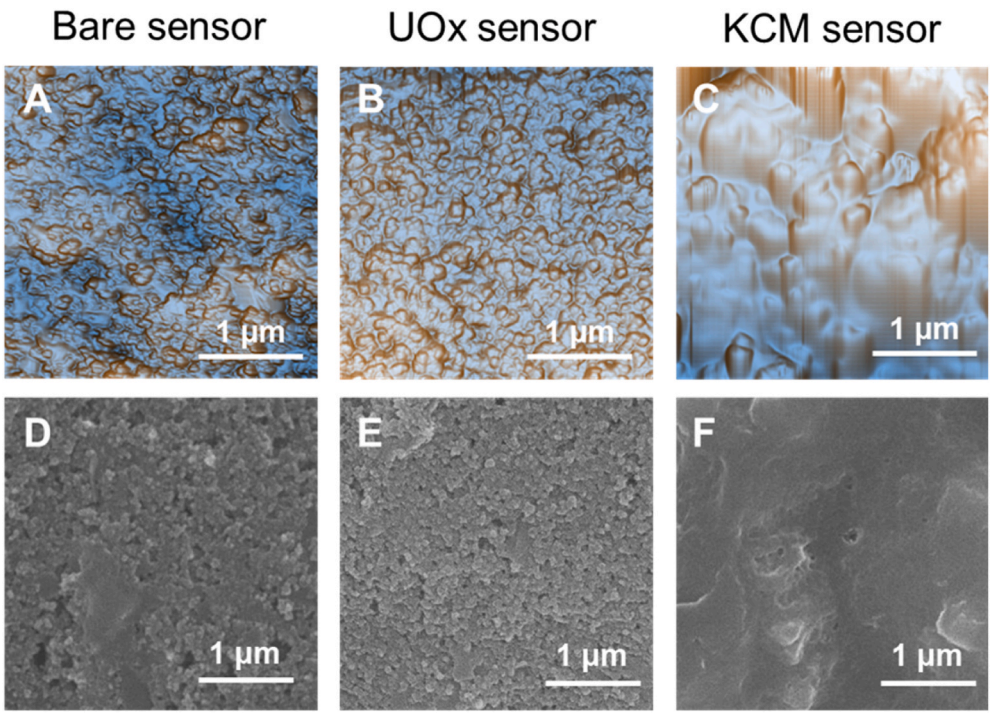

Fig. 1. AFM images of (A) bare, (B) UOx, and (C) KCM sensors. SEM images of (D) bare, (E) UOx, and (F) KCM sensors.

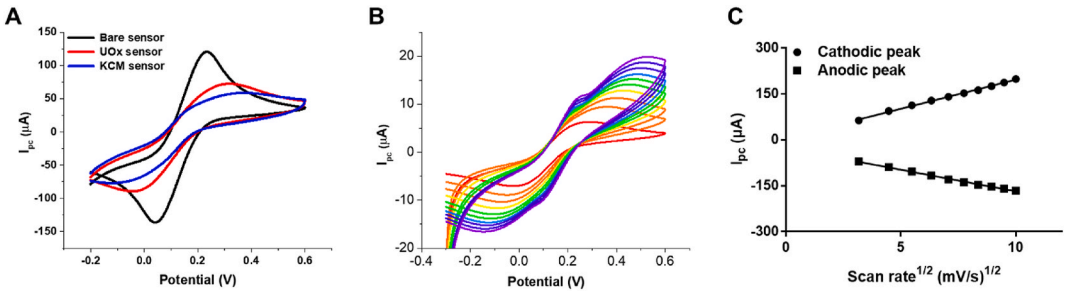

Fig. 2. (A) CV of bare, UOx, and KCM sensors at a scan rate of 50 mV/s and scan range of −0.2 to 0.6 V in PBS (pH 7.4) containing 0.2 M KCl and 10 mM $[Fe(CN)_6]^{3-/4-}$. (B) CV of the KCM sensor at a scan rate of 10–100 mV/s in PBS (pH 7.4) containing 0.2 M KCl and 10 mM $[Fe(CN)_6]^{3-/4-}$. (C) Plot of peak current versus square root of scan rate. The linear correlation coefficients of I_{pc} and I_{pa} were 0.9944 and 0.9935, respectively.

selected antioxidants. The I_{pc} values of the KCM sensor for the UA–antioxidant solutions were highly consistent, with errors of only 0.22%–1.7%. On the other hand, the I_{pc} of the UOx sensor showed 3.38–14.9% error in the presence of antioxidants, owing to the electrochemical interference produced by each antioxidant. The deviations of the UOx sensor for AA, BA, GSH, LA, and NA were 24.3, 9.4, 22.0, 6.1, and 9.6% larger than that of the KCM sensor, respectively. These results demonstrate the permselectivity of the KCM sensor with URAT1 and the phospholipid bilayer. The mechanism of permselectivity can therefore be explained through two mechanisms: i) URAT1 selectively transports UA across the KCM, and ii) the phospholipid bilayer of KCM prevents antioxidants from permeating through the membrane.

3.6. Feasibility, stability, and reproducibility of the KCM sensor

We tested the feasibility of the KCM sensor in the presence of UA solubilized in 0.1 × human serum (Fig. 5A). The amount of UA in the 0.1 × human serum (34.9 μM) was measured using a UA assay kit (Fig. S8). Although the sensitivity of the KCM sensor decreased when UA was measured in the serum, the I_{pc} linearly increased with the concentration of UA. The coefficient of determination was 0.9839. We also determined the stability of the sensor after three weeks of storage by measuring UA (Fig. 5B).

After 3 weeks of storage, the KCM sensor showed an I_{pc} of 100 ± 1.0% compared to that of a freshly made KCM sensor. This result demonstrates that the enzymatic activity of UOx and the UA transportation capability of URAT1 was stable for three weeks. The stability of cell membranes coated on solid surfaces was also investigated in our previous study (Kim et al. 2019, 2020, 2021). Furthermore, we tested the selectivity of the KCM sensor after three weeks of storage. After testing the UA and BA mixture, the I_{pc} of the KCM sensor stored for 3 weeks was 100 ± 0.3% of that of a freshly prepared KCM sensor. It was therefore verified that the selectivity derived from KCM was retained after 3 weeks of storage. Reproducibility was assessed by comparing the activity of independently fabricated KCM sensors (Fig. 5C). The deviation for each sensor ranged from 0.5 to 1.6% for 400 μM UA, indicating that the electrochemical properties of the independently fabricated KCM sensors were highly consistent.

4. Conclusion

We developed a highly selective UA biosensor using URAT1-rich KCM as a permselective filter. The KCM coating on the enzymatic sensor was verified through surface visualization and topological

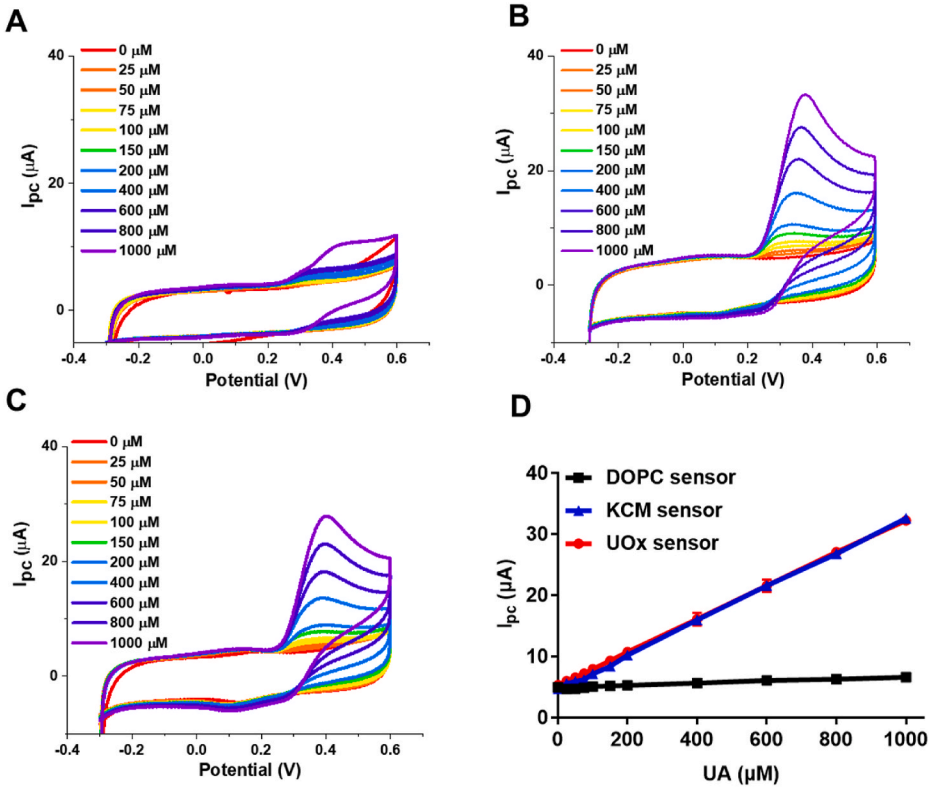

Fig. 3. CV of (A) DOPC, (B) UOx, and (C) KCM sensors for 0–1000 μM UA at a scan rate of 50 mV/s. (D) Plots of I_{pc} for each sensor versus UA concentration obtained from (A–C).

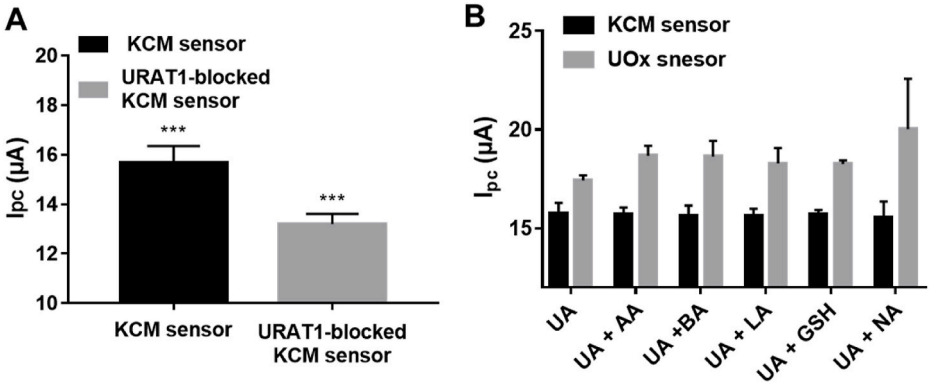

Fig. 4. (A) I_{pc} of KCM and URAT1-blocked KCM sensors for 400 μM UA. (***$p \leq 0.001$, n = 4 for each sensor; significance was determined through one-way ANOVA). (B) Selectivity of the KCM sensor for measuring 400 μM UA mixed with 40 μM of each antioxidant (AA: ascorbic acid, BA: barbituric acid, LA: lipoic acid, GSH: glutathione, and NA: niacinamide).

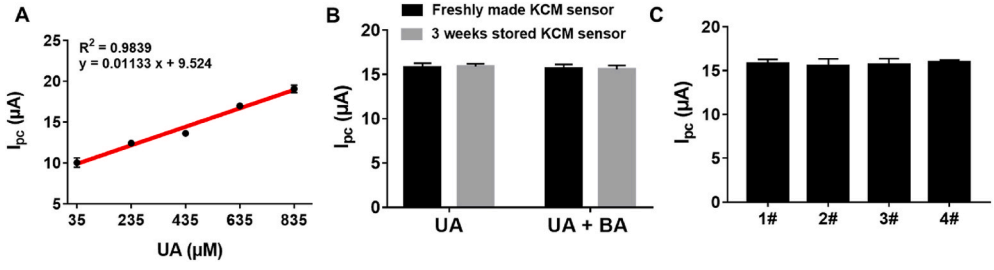

Fig. 5. (A) UA detection in the human serum using KCM sensors to verify its feasibility. (B) Stability of the KCM sensor for detecting 400 μM UA with or without 40 μM BA. The I_{pc} of freshly made and 3 week-old KCM sensors were highly similar. (C) Reproducibility of four batches of KCM sensors verified with 400 μM UA.

analysis. It was confirmed, by comparing the KCM and DOPC sensors, that URAT1 is a key factor in transporting UA to UOx immobilized on the sensor electrode. Furthermore, the UA permeation capability of URAT1 was demonstrated through its inhibition. The KCM sensor was permselective to UA and was unaffected by the five major antioxidants in the blood. The KCM sensor detected UA in the range of 0–1000 μM, with a limit of detection of 8.5 μM, suggesting its application in the diagnosis of early stage gout. In addition, the KCM sensor demonstrated feasibility in measuring UA in human serum, exhibiting high reproducibility. Finally, the KCM sensor was stable for three weeks, retaining its permselectivity for UA. The sensitivity of the fabricated sensor, however, needs to be increased for clinical applications. Further, possible interference from other types of interfering molecules, such as proteins and ions, should be confirmed in future work. Nonetheless, the KCM sensor could be potentially applicable for the early diagnosis of gout as a point-of-care test.

CRediT authorship contribution statement

Insu Kim: Investigation, Conceptualization, Methodology, Writing, Formal analysis, Writing – original draft, Cell membrane extraction. **Young Im Kim:** Investigation, Methodology, Visualization, Writing – review & editing. **Sang Won Lee:** Cell culture. **Hyo Gi Jung:** Visualization. **Gyudo Lee:** Writing – review & editing. **Dae Sung Yoon:** Supervision, Writing – review & editing.

Declaration of competing interest

The authors declare that they have no known competing financial interests or personal relationships that could have appeared to influence the work reported in this paper.

Acknowledgments

This work was supported by the National Research Foundation of Korea (NRF) Grant funded by the Korean Government (MSIP) (No., NRF-2018M3C1B7020722, NRF-2019R1A2B5B01070617, and 2020R1A6A3A01096477). This work was supported by the Korea Medical Device Development Fund grant funded by the Korea government (the Ministry of Science and ICT), Project Number: 202012D19. This study was also supported by the BK21 FOUR (Fostering Outstanding Universities for Research).

Appendix A. Supplementary data

Supplementary data to this article can be found online at https://doi.org/10.1016/j.bios.2021.113411.

References

Abou-Elela, A., 2017. J. Adv. Res. 8 (5), 513–527.
Bacellar, I.O., Baptista, M.S., Junqueira, H.C., Wainwright, M., Thalmann, F., Marques, C.M., Schroder, A.P., 2018. Biochim. Biophys. Acta 1860 (11), 2366–2373.
Elgrishi, N., Rountree, K.J., McCarthy, B.D., Rountree, E.S., Eisenhart, T.T., Dempsey, J. L., 2018. J. Chem. Educ. 95 (2), 197–206.
Fitz-Patrick, D., Roberson, K., Niwa, K., Fujimura, T., Mori, K., Hall, J., Yan, X., Shen, Z., Liu, S., Ito, Y., 2018. Mod. Rheumatol. 29 (6), 1042–1052.
Ghosh, T., Sarkar, P., Turner, A.P.F., 2015. Bioelectrochemistry 102, 1–9.
Hedegaard, S.F., Derbas, M.S., Lind, T.K., Kasimova, M.R., Christensen, M.V., Michaelsen, M.H., Campbell, R.A., Jorgensen, L., Franzyk, H., Cárdenas, M., Nielsen, H.M., 2018. Sci. Rep. 8 (1), 6327. https://doi.org/10.1038/s41598-018-24154-z.
Jo, S., Kim, I., Lee, W., Kim, M., Park, J., Lee, G., Yoon, D.S., Park, J., 2019. Biosens. Bioelectron. 135, 216–223.
Kim, I., Kim, C., Lee, D., Lee, S.W., Lee, G., Yoon, D.S., 2020. Analyst 145 (6), 2125–2132.
Kim, I., Kim, Y., Lee, S.W., Lee, D., Jung, H.G., Jang, J.W., Lee, T., Yoon, Y.K., Lee, G., Yoon, D.S., 2021. Biosens. Bioelectron. 185, 113267 https://doi.org/10.1016/j.bios.2021.113267.
Kim, I., Kwon, D., Lee, D., Lee, G., Yoon, D.S., 2019. Biosens. Bioelectron. 135, 82–87.
Kim, I., Kwon, D., Lee, D., Lee, T.H., Lee, J.H., Lee, G., Yoon, D.S., 2018. Biosens. Bioelectron. 102, 617–623.
Krishnan, S.K., Singh, E., Singh, P., Meyyappan, M., Nalwa, H.S., 2019. RSC Adv. 9, 8778–8881.
Lee, T., Kim, I., Cheong, D.Y., Roh, S., Jung, H.G., Lee, S.W., Kim, H.S., Yoon, D.S., Hong, Y., Lee, G., 2021. Anal. Chim. Acta 1158, 338387. https://doi.org/10.1016/j.aca.2021.338387.
Mathew, M., Radhakrishnan, S., Vaidyanathan, A., Chakraborty, B., Rout, C.S., 2021. Anal. Bioanal. Chem. 413 (3), 727–762.
Perry, J.L., Dembla-Rajpal, N., Hall, L.A., Pritchard, J.B., 2006. J. Biol. Chem. 281 (49), 38071–38079.
Price, D.W., Warren, G.W., Drouven, B., 1986. J. Appl. Electrochem. 16 (5), 719–731.
RoyChoudhury, S., Umasankar, Y., Hutcheson, J.D., Lev-Tov, H.A., Kirsner, R.S., Bhansali, S., 2018. Electroanalysis 30 (10), 2374–2385.
Shi, K., Shiu, K.-K., 2001. Electroanalysis 13 (16), 1319–1325.
Shindyapina, A.V., Komarova, T.V., Sheshukova, E.V., Ershova, N.M., Tashlitsky, V.N., Kurkin, A.V., Yusupov, I.R., Mkrtchyan, G.V., Shagidulin, M.Y., Dorokhov, Y.L., 2017. Front. Neurosci. 11, 651. https://doi.org/10.3389/fnins.2017.00651.
Singh, G., Lingala, B., Mithal, A., 2019. Rheumatology 58 (12), 2177–2180.
Stiburkova, B., Bohata, J., Minarikova, I., Mancikova, A., Vavra, J., Krylov, V., Doležel, Z., 2019. Appl. Sci. 9 (17), 3479. https://doi.org/10.3390/app9173479.
Tan, P.K., Liu, S., Gunic, E., Miner, J.N., 2017. Sci. Rep. 7 (1), 665. https://doi.org/10.1038/s41598-017-00706-7.
Vaidya, B., Bhochhibhoya, M., Nakarmi, S., 2018. Biomed. Rep. 9 (1), 60–64.
Wang, J., Pedrero, M., Sakslund, H., Hammerich, O., Pingarron, J., 1996. Analyst 121 (3), 345–350.
Yan, Q., Zhi, N., Yang, L., Xu, G., Feng, Q., Zhang, Q., Sun, S., 2020. Sci. Rep. 10 (1), 0607 https://doi.org/10.1038/s41598-020-67394-8.